iScience

CellPress
OPEN ACCESS

Article

FXN targeting induces cell death in ovarian cancer stem-like cells through PRDX3-Mediated oxidative stress

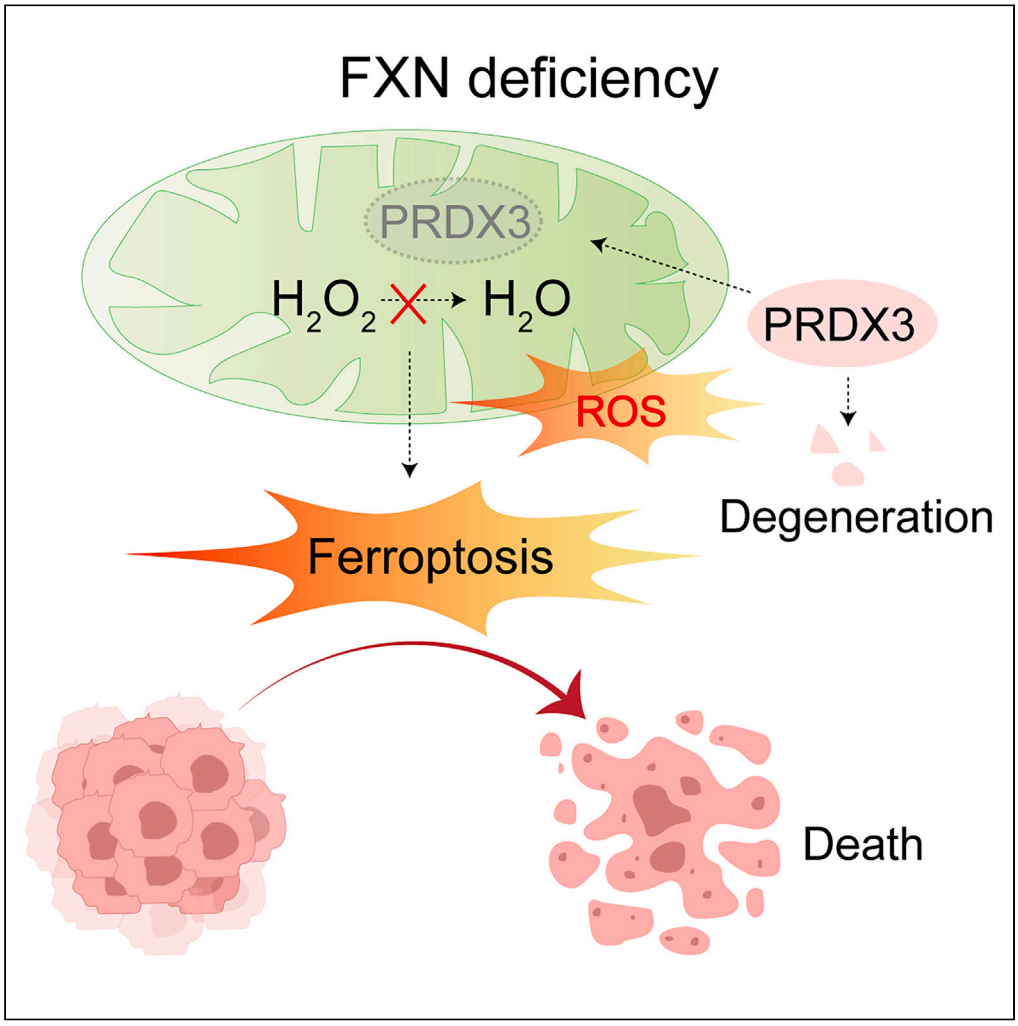

Shanshan Xu, Yuwan Liu, Shizhou Yang, Weidong Fei, Jiale Qin, Weiguo Lu, Junfen Xu

xjfzu@zju.edu.cn

Highlights

High expression of FXN in OCSLCs is associated with poor prognosis

FXN deficiency suppresses OCSLCs stemness and viability

Loss of FXN triggers PRDX3-mediated oxidative stress

FXN inhibition enhances the degeneration of PRDX3

Xu et al., iScience 27, 110506
August 16, 2024
https://doi.org/10.1016/j.isci.2024.110506

iScience

CellPress
OPEN ACCESS

Article

FXN targeting induces cell death in ovarian cancer stem-like cells through PRDX3-Mediated oxidative stress

Shanshan Xu,[1] Yuwan Liu,[2] Shizhou Yang,[1] Weidong Fei,[3] Jiale Qin,[4] Weiguo Lu,[1,5] and Junfen Xu[1,5,6,*]

SUMMARY

Ovarian cancer stem cells (OCSCs) significantly impact the prognosis, chemoresistance, and treatment outcomes in OC. While ferroptosis has been proven effective against OCSCs, the intricate relationship between ferroptosis and OCSCs remains incompletely understood. Here, we enriched ovarian cancer stem-like cells (OCSLCs) through mammosphere culture, as an OCSC model. OCSLCs displayed heightened ferroptosis susceptibility, correlating with elevated FXN levels compared to non-stem OC cells. FXN has recently emerged as a potential regulator in ferroptosis. FXN knockdown diminished stemness marker nanog, sphere-forming ability, increased reactive oxygen species (ROS) generation, and attenuated OCSLCs viability. FXN overexpression exacerbated ferroptosis resistance and reduced RSL3-induced cell death. FXN knockdown impeded OCSLC xenograft tumor growth and exacerbated the degeneration of peroxiredoxin 3 (PRDX3), a mitochondrial antioxidant protein participates in oxidative stress. Thus, elevated FXN in OCSLCs suppresses ROS accumulation, fostering ferroptosis resistance, and regulates the antioxidant protein PRDX3. FXN emerges as a potential therapeutic target for OC.

INTRODUCTION

Ovarian cancer stands as one of the most formidable challenges in the realm of female reproductive system cancers, projecting approximately 19,710 new cases and 13,270 deaths expected in the United States in 2023.[1,2] Although initial responses to standard treatment, including debulking surgery and platinum-based chemotherapy with or without targeted maintenance therapy,[3] are promising, the recurrence of chemoresistant phenotype in about 80% of ovarian cancer patients poses a significant hurdle.[4] Consequently, the 5-year overall survival (OS) rate languishes at only 30%.[5] The pervasive issue of drug resistance in ovarian cancer underscores the urgency for innovative therapeutic approaches.[6]

Recently, increasing evidence has shown that ovarian cancer chemoresistance is mainly due to oxidative stress and ferroptosis resistance.[7] Ferroptosis, a non-apoptotic cell death mechanism reliant on intracellular iron and characterized by the accumulation of lipid reactive oxygen species (ROS), has demonstrated heightened efficacy in inducing ovarian cancer cells death. Sonia Fantone et al. reported that SLC7A11 expression was increased in ovarian cancer tissues in which it could inhibit ferroptosis and favor cancer cell chemoresistance, suggesting a possible therapeutic target.[8] Notably, accumulating evidence suggests that cancer stem cells (CSCs), a minute subset within tumors endowed with self-renewal, tumor-initiating capabilities, and chemoresistance, exhibit greater susceptibility to ferroptosis compared to non-CSCs in various cancers, including breast and esophageal cancer.[9,10] Despite promising research on targeting CSCs to enhance cancer treatment efficacy,[4,11] challenges persist as the underlying mechanisms remain elusive, and optimal treatments targeting CSCs are yet to be realized.[12] Recent data demonstrate that ferroptosis inducers could specifically target CSCs,[13] offering a fresh perspective in the battle against ovarian cancer. This discovery underscores the potential of ferroptosis in achieving complete tumor eradication and overcoming chemotherapy resistance.[9] Several agents, such as erastin, frizzled-7, superparamagnetic iron oxide nanoparticles, and stearoyl-coenzyme A desaturase 1 (SCD1), have shown promise in specifically targeting ovarian cancer stem cells (OCSCs) through ferroptosis induction.[14–16] However, challenges persist as the mechanisms governing ferroptosis in OCSCs are not fully understood, and the treatments developed are not yet optimal. Therefore, the exploration of ferroptosis induction as a strategy to combat OCSCs and improve the clinical outcome is gaining considerable attention.

[1]Department of Gynecologic Oncology, Women's Hospital, Zhejiang University School of Medicine, Hangzhou 310006, Zhejiang, China
[2]Women's Reproductive Health Laboratory of Zhejiang Province, Women's Hospital, Zhejiang University School of Medicine, Hangzhou 310006, Zhejiang, China
[3]Department of Pharmacy, Women's Hospital, Zhejiang University School of Medicine, Hangzhou 310006, Zhejiang, China
[4]Department of Ultrasound, Women's Hospital, Zhejiang University School of Medicine, Hangzhou 310006, Zhejiang, China
[5]Zhejiang Provincial Clinical Research Center for Obstetrics and Gynecology, Hangzhou 310006, Zhejiang, China
[6]Lead contact
*Correspondence: xjfzu@zju.edu.cn
https://doi.org/10.1016/j.isci.2024.110506

Frataxin (FXN, coded by FXN gene: LRG_339), a highly conserved mitochondrial protein primarily involved in mitochondrial iron-sulfur clusters biosynthesis and cellular iron homeostasis, has recently emerged as a potential player in ferroptosis.[17] FXN deficiency could contribute to mitochondrial iron accumulation,[17,18] increased ROS production, and lipid peroxidation,[19,20] all characteristic features of ferroptosis. Jing Du had certified FXN as a negative regulator of ferroptosis,[21] with its deficiency significantly increasing susceptibility to ferroptosis.[20] Interestingly, FXN deficiency has been associated with decreased expression of ferroptosis negative regulators, including glutathione peroxidase 4 (GPX4) and NFE2 like bZIP transcription factor 2 (NRF2).[20,22] Moreover, a recent finding proposes FXN as a key regulator of ferroptosis in fibrosarcoma, suggesting its potential as a therapeutic target.[21] However, the specific role of FXN in ferroptosis within OCSCs remains unclear.

In previous studies, we successfully enriched OCSCs in mammosphere culture, denoted as spheroids or ovarian cancer stem-like cells (OCSLCs). These OCSLCs exhibited phenotypic characteristics of OCSCs, showing high expression of stem marker Nanog and sphere-forming ability.[23,24] Building upon this foundation, OCSLCs were employed as a model for OCSCs in the current study. Here, we unveil that FXN is highly expressed in ovarian cancer, correlating with poor progress. Furthermore, FXN is upregulated in OCSLCs compared to parental cells. Importantly, depletion of FXN induces ferroptosis in OCSLCs through active oxygen species (ROS) accumulation, leading to the inhibition of self-renewal and cell viability. Subsequent investigations reveal that FXN inhibition disrupts intracellular redox homeostasis by enhancing the degeneration of peroxiredoxin 3 (PRDX3). Collectively, FXN deficiency emerges as a promising candidate for ovarian cancer treatment, exerting its effects through ferroptosis induction via the targeting of PRDX3.

RESULTS

FXN predicts poor progression in ovarian cancer

In a recent study, Mohammad Ghazizadeh reported elevated frataxin expression in cisplatin-resistant A2780 cells ($A2780^{CR}$) compared to parental A2780 cells,[25] a finding validated through western blot analysis in our study (Figure 1A). The heightened expression of FXN in $A2780^{CR}$ prompted an investigation into its association with ovarian cancer progression and poor prognosis, especially considering the urgency in addressing cisplatin resistance, a crucial factor in ovarian cancer treatment. Our analysis revealed an increased level of FXN protein in ovarian cancer tissues compared to normal ovarian epithelium tissues (Figure 1B). Further examination of FXN mRNA expression using http://kmplot.com based on 614 ovarian cancer patients, in which 188 patients with high FXN expression demonstrating poor progression-free survival (PFS) (Figure 1C).

To establish the clinical relevance of FXN in ovarian cancer, immunohistological (IHC) analysis of FXN protein expression was performed in 178 ovarian cancer tissues comprising patient samples and investigated the correlation between FXN expression and clinical parameters. The IHC results showed a significant association between elevated FXN levels and advanced Federation International of Gynecology and Obstetrics (FIGO) stage, higher tumor grade, and increased serum CA125 (Table 1). Moreover, FXN staining was significantly higher in high-stage ovarian cancers relative to low-stage patients (Figure 1D). Importantly, patients with high FXN IHC scores were associated with poor PFS and OS (Figure 1E). These findings suggest that FXN could be a potential therapeutic target for ovarian cancer.

FXN regulates cells viability and cancer stem-like cell characteristics via oxidative stress-mediated ferroptosis

To gain insight into mechanisms of FXN in ovarian cancer, we analyzed the gene effect score for FXN in ovarian cancer cell lines using DepMap (Figure S1A), selecting Skov3 and Ovcar5 cell lines for further investigation. Compared to normal human ovarian surface epithelial (HOSE) cells, there was an increase in the level of FXN proteins in Skov3 and Ovcar5 spheroids (Figure S1B). In addition, western blot analysis revealed elevated levels of both FXN and stemness marker Nanog in OCSLC spheroids compared to parental cells (Figure 2A). Notably, OCSLCs exhibited increased susceptibility to ferroptosis, as evidenced by higher cell death upon exposure to the ferroptosis-inducers RSL3 or erastin (Figure 2B). Given the established link between FXN and cellular iron homeostasis, ROS production, and ferroptosis,[18,19,26] we explored the potential connection in ovarian cancer stem-like cells. Our data indicated that FXN expression attenuated with the increase of ferroptosis-inducer RSL3, a covalent inhibitor of the GPX4 enzymatic activity (Figure 2C), suggesting a possible link between FXN and ferroptosis in OCSLCs.

To explore the functional roles of FXN, we utilized FXN siRNAs with two independent sequences and performed experiments in mammosphere culture. The cells depleted of FXN exhibited a significant decrease in the stem cell related-marker Nanog compared to the control cells (Figure 2D). Moreover, we observed a concurrent reduction in sphere-forming ability upon FXN knockdown (Figure 2E). Consistent with these findings, FXN deficiency negatively impacted cell viability, as evidenced by cell viability assay results (Figure 2F). Considering recent study reported that FXN deficiency is accompanied by higher levels of p53.[27,28] In line with these, we verified P53 was negatively linked with FXN expression (Figure S1C). Given that an elevated production of ROS is a distinctive hallmark of ferroptosis, our investigations revealed an increase in lipid ROS levels in Skov3 and Ovcar5 OCSLCs upon FXN depletion, as assessed by lipid ROS assay (Figure 2G). Additionally, we noted an upregulation of transferrin receptor (TFR1), an iron-responsive element encoding protein, in conjunction with FXN deficiency (Figure 2H). Conversely, we generated pooled FXN-overexpression cells, confirming their efficiency through mRNA and protein analyses (Figure 3A). These cells exhibited enhanced cell viability (Figure 3B) and decreased cell death (Figure 3C), accompanied with lower level of ROS (Figure 3D) and TFR1 protein expression (Figure 3E) compared to OCSLCs containing an empty vector. In addition, FXN overexpression exacerbated resistance to ferroptosis, reducing cell death induced by RSL3 using cell viability assay and calcein-AM/propidium iodide (PI) staining assay (Figures 3F and 3G). Collectively, these findings suggest that inhibiting FXN could reduce cell viability and cancer stem-like cell properties, potentially through oxidative stress-mediated ferroptosis.

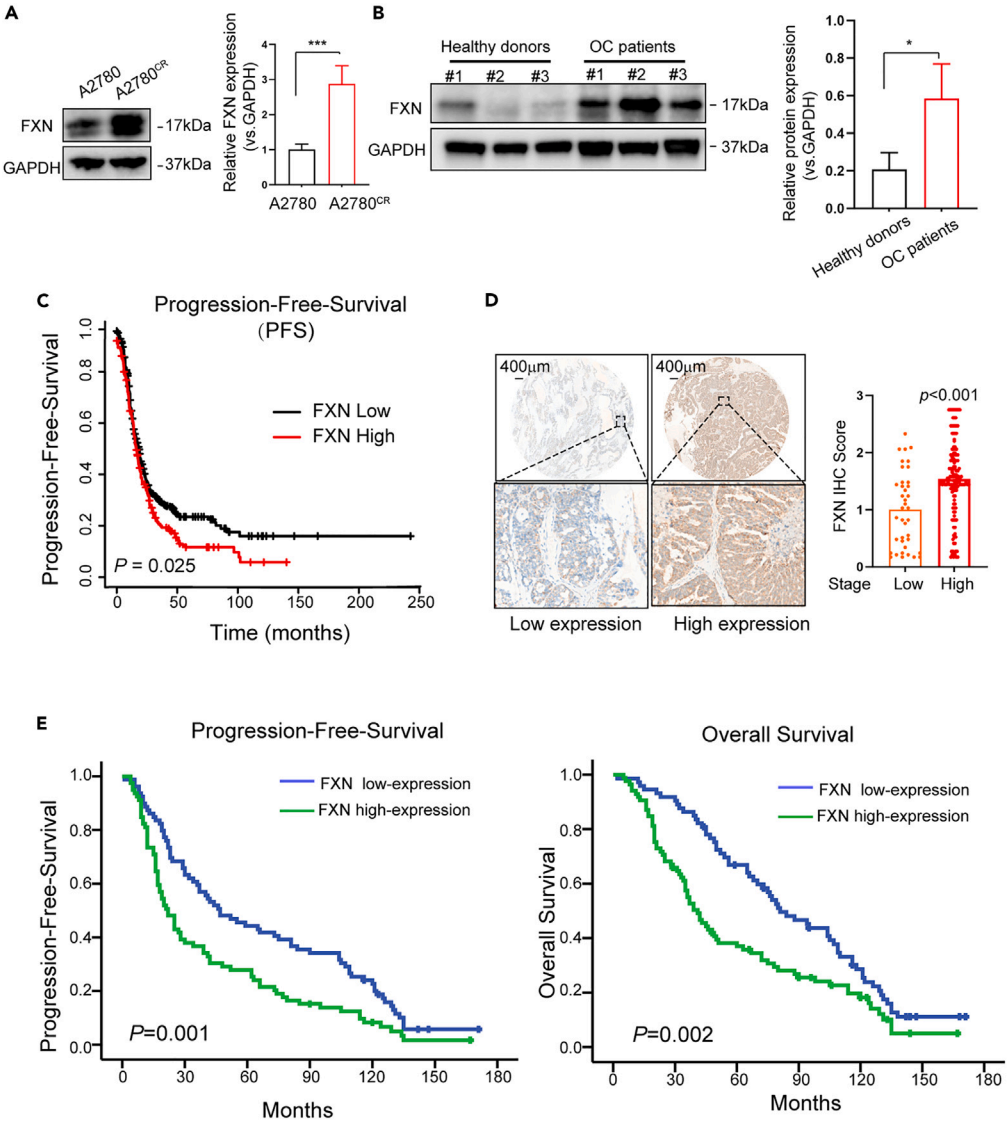

Figure 1. FXN predicts poor progression in ovarian cancer

(A) Immunoblot (IB) showing the expression of FXN in cisplatin-resistant A2780 cells and the parental A2780 cells (mean ± S.E., $n = 3$, biologically independent experiments).

(B) IB showing the levels of FXN in OC tissues and the normal ovarian tissues (N = normal, C = cancer).

(C) Kaplan–Meier plots of progression-free survival for OC samples ($n = 614$) from the KM Ploter database on Affymetrix id 230234_at.

(D and E) Immunohistochemical staining was performed using specific primary anti-FXN antibody in ovarian cancer tissues. Representative images and boxplots of histoscore of FXN in low stage and high stage ovarian cancer tissue is shown (D). Scale bars, 400 μm. (low stage, $n = 39$; high stage, $n = 139$). Kaplan-Meier survival analysis of patients with FXN low ($n = 90$) and FXN high ($n = 88$) expression in ovarian cancer are shown (E).

See also Figure S1 and Table S1.

PRDX3 is a downstream target of FXN in ovarian cancer stem-like cells

In view of the exact mechanism accounting for FXN involved in ferroptosis regulation requires further evaluation, liquid chromatography-tandem mass spectrometry (LC-MS/MS) analysis on Ovcar5 spheroids with either control or FXN knockdown were performed. Gene comparison of differentially expressed proteins ($|\log_2 FC|>1.2$, $p < 0.05$; Figure 4A; Table S1) of the siFXN and negative control samples revealed 104 proteins associated with various biological processes. Gene ontology (GO) analysis of these differentially expressed genes indicated a significant downregulation of proteins involved in the hydrogen peroxide catabolic process upon FXN depletion (Figure 4B). Immunoblotting analysis confirmed the downregulation of PRDX3, a key protein in the hydrogen peroxide catabolic process and a marker for ferroptosis,[29] in both Skov3 and Ovar5 cell lines (Figure 4C). PRDX3, a thioredoxin-dependent peroxide reductase family of mitochondrial antioxidant protein, play a crucial role in the response to oxidative stress, catalyzing the reduction of both hydrogen peroxide and

Table 1. Association of FXN expression with clinicopathological characteristics in ovarian cancer patients (*n* = 178)

Variable	All cases,N(%)	FXN expression		*p* value
		Low	High	
Age(years)				0.513
≦50	70(39.3)	35	35	
>50	108(60.7)	55	53	
FIGO stage				0.001**
I/II	39(21.9)	29	10	
III/IV	139(78.1)	61	78	
Tumor grade				0.011*
I/II	60(33.7)	38	22	
III	118(66.3)	52	66	
Ascitic fluid volume(ml)				0.067
<500	106(59.6)	59	47	
≥500	72(40.4)	31	41	
Serum CA125(U/ml)				0.035*
<500	86(48.3)	50	36	
≥500	92(51.7)	40	52	

χ^2 test, $^{**}p < 0.01$, $^{*}p < 0.05$.
See also Table S2.

alkyl peroxides to water.[30] So far, many studies have revealed the inner link between PRDX3 and ferroptosis. For instance, it was reported that PRDX3 could cause cells resistance to ferroptosis (Cui et al.),[29] participate in aminolevulinic acid mediated ferroptotic cell death (Lynch et al.),[31] and regulate ferroptosis associated with ROS production via GPX4/SLC7A11 pathway (Wang et al.).[32] For these considerations, PRDX3 downregulation following FXN deficiency could be a desirable occurrence since it could also suggest increased ROS in ovarian cancer stem-like cells following FXN silencing. To assess whether PRDX3 is an effective target of FXN, we established cell lines harboring silenced PRDX3 siRNA gene expression and analyzed the viability of cancer stem-like cells and ROS level. Interestingly, we observed a significant increase in cell death in siPRDX3-transfected cells compared to controls, corresponding to a dramatical ascension in ROS levels (Figures 4D–4F), indicating that PRDX3 knockdown enhances cell death via oxidative stress. We further investigated whether FXN silencing induced cell death and ROS production could be attributed to PRDX3. OCSLCs with FXN depletion were cultured either alone or in combination with a PRDX3 overexpressing plasmid, and cell viability along with lipid ROS levels was assessed. The results demonstrated that FXN silencing-induced cell death and ROS accumulation could be rescued by PRDX3 overexpression (Figures 4G–4I), providing additional support for the hypothesis that ferroptosis induced by FXN inhibition may occur through PRDX3-mediated oxidative stress.

FXN stabilizes PRDX3 by inhibiting its proteasome degradation

Next, we examined whether FXN regulates the mRNA or protein levels of PRDX3. The levels of PRDX3 were assessed through qPCR analysis and western blot. The results showed that silencing FXN led to a decrease in PRDX3 protein levels without affecting PRDX3 mRNA levels (Figure 5A). Additionally, we explored whether FXN influenced the stability of PRDX3 protein. Cycloheximide, a protein synthesis inhibitor, was employed to assess the impact of FXN on PRDX3 stability. Cells transfected with FXN siRNAs were treated with 50 μg/mL CHX for various durations to block protein synthesis. The degradation rates of existing PRDX3 protein were measured by western blot. The results indicated that FXN depletion exacerbated PRDX3 degradation compared to the control group (Figure 5B). To further establish the relationship between PRDX3 degradation and FXN, we treated cells with MG132, a proteasome inhibitor, or chloroquine, a lysosomal acidification inhibitor. The results showed that treatment with MG132, but not chloroquine, led to an accumulation of PRDX3 protein (Figure 5C). This suggests that the proteasome pathway may be required for PRDX3 reduction caused by FXN deletion. This finding is consistent with the report by Huang et al., who proposed the involvement of the ubiquitin-proteasome pathway in modulating PRDX3 stability.[33]

FXN deficiency markedly impeded tumor growth in an ovarian tumor xenograft mouse model

To assess the *in vivo* tumor-initiating potential, Skov3 cells were transduced with short hairpin RNAs targeting FXN or scramble sequences, and cultured for anchorage-independent growth. After 7 days, spheroid cells (1*10^6) were injected into the axillary region of BALB/c-nu mice. Tumor development was monitored in the control group seven days post-injection, with subsequent measurements of tumor diameter

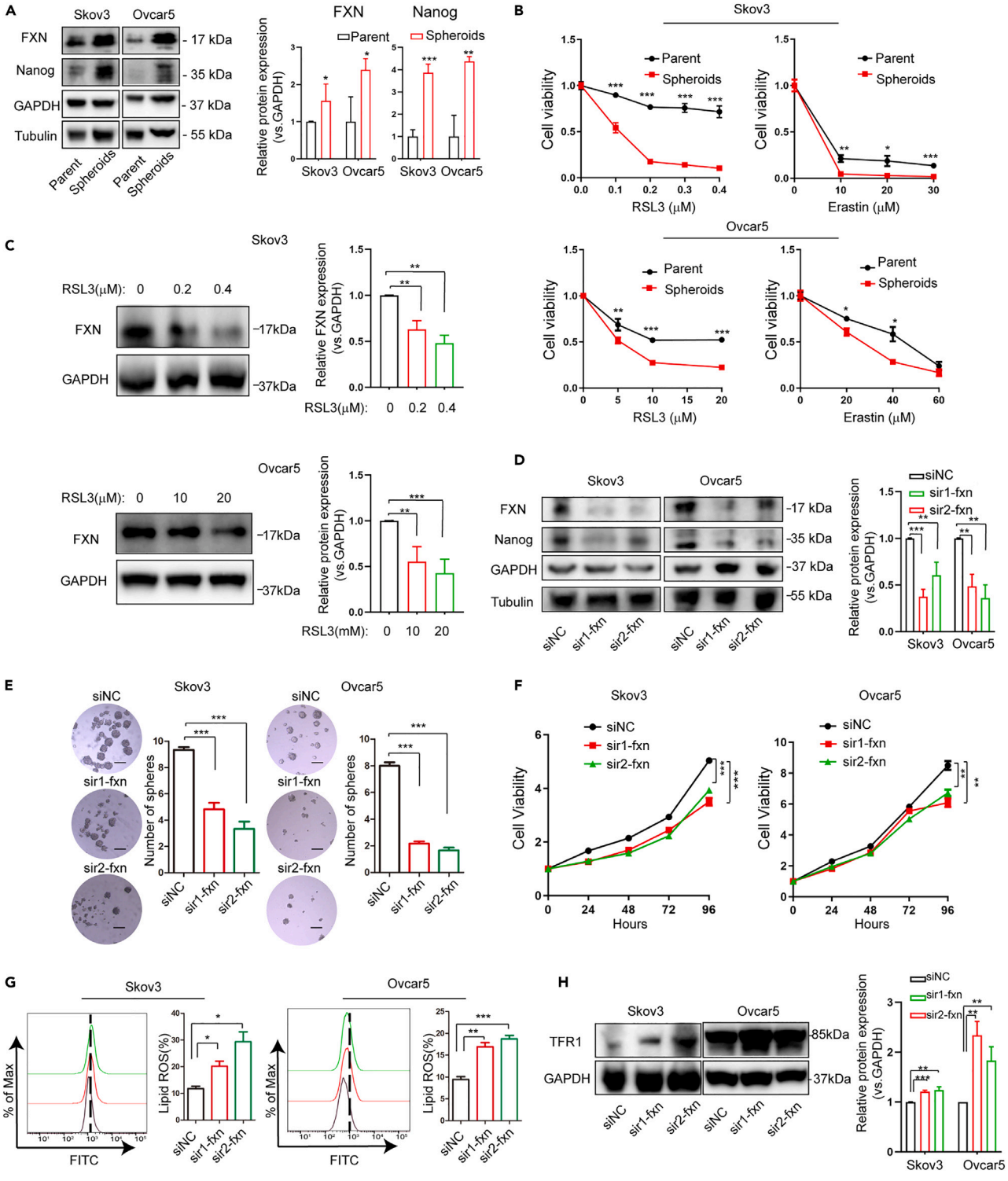

Figure 2. FXN knockdown inhibits cells viability and cancer stem-like cell characteristics via oxidative stress-mediated ferroptosis

(A) IB showing the expression of FXN and stem-cell marker Nanog in parent and spheroid cells (mean ± S.E., *n* = 3, biologically independent experiments).

(B) CCK8 assay analyzed the cell viability between parent and spheroids treated with Erastin or RSL3 in skov3 and Ovcar5 cell lines, respectively (*n* = 3).

(C) IB showing the levels of FXN in Skov3 and Ovcar5 spheroids treated with RSL3 for 24 h (Skov3 with 0, 0.2μm, and 0.4μm, Ovcar5 with 0, 10μm, and 20μm, respectively) (mean ± S.E., *n* = 3, biologically independent experiments).

Figure 2. *Continued*

(D–H) FXN knockdown (KD) spheroids were generated by siRNA system. IB illustrating the levels of indicated proteins in Ctrl and FXN-depleting spheroids (D). (mean ± S.E., $n = 3$, biologically independent experiments). Quantifications of tumorsphere numbers (1000 cells/well) formed by Ctrl or FXN KD spheroids (2E, right) (mean ± S.E., $n = 3$, biologically independent experiments). Representative images of tumorspheres are shown (2E, left). Scale bar, 100 μm. Cell growth was assessed in Ctrl and FXN deficiency spheroids, respectively ($n = 3$) (F). The lipid ROS levels, as indicated by DCFDA fluorescence, were measured by flow cytometry in FXN KD and Ctrl spheroids (G) (Mean ± S.E., $n = 3$, biologically independent experiments). Immunoblot illustrating the levels of TFR1 protein in the indicated spheroids (H) (Mean ± S.E., $n = 3$, biologically independent experiments). Statistical significance was assessed by paired t test. *$p < 0.05$, **$p < 0.01$, ***$p < 0.001$.

See also Figure S1.

every 7 days. Remarkably, no tumors were observed in the FXN downregulated group even after four weeks. The figure illustrates a significant reduction in the tumor-initiating capacity of FXN deficient cells in mice compared to the control group (Figure 5D). These findings strongly indicate that FXN knockdown suppresses tumor-initiating capacity.

DISCUSSION

The last few decades have witnessed exceptional breakthroughs in cancer therapy. Unfortunately, although many new therapeutic strategies have been developed to battle cancer, such as target therapy,[34] immunotherapy,[35,36] drug resistance, there is remaining the main limitation for achieving cures in cancer patients. One major cause is the existence of CSCs, a small subset of cells within tumors,[36] have been identified in various cancer types and pose challenges for effective treatment strategies.[11,37–39] Despite efforts to target CSCs through various approaches, including disrupting redox homeostasis and modulating signaling pathways,[40] optimal treatments are yet to be realized. Ferroptosis, a form of regulated cell death, has emerged as a potential avenue for eradicating CSCs in different cancer types.[41] Previous studies have shown sensitivity of OCSCs to ferroptosis inducers like erastin.[42] Based on 3D spheroids model already widely adopted in our laboratory, we contribute to this understanding by demonstrating that FXN, a mitochondrial protein upregulated in OCSLCs, plays a role in modulating ferroptosis. Mechanistically, FXN deficiency promotes PRDX3 degradation, increases ROS levels, and accelerates ferroptosis and cell death in OCSLCs (Figure 5E).

FXN is known for its role in cellular iron homeostasis, involving mitochondrial iron import, storage, and ferritinophagy. The literature has linked FXN deficiency to increased oxidative stress and iron accumulation, resembling hallmarks of ferroptosis.[43] For instance, Campanella and collaborators found that the overexpression of mitochondrial ferritin (FTMt), responsible for iron import from the cytosol into the mitochondrion, decreases ROS production and partially recover mitochondrial enzyme activities in FXN-deficient patients.[44] Despite evidence linking FXN to ferroptosis, especially in cancers, remains elusive only Du reported that FXN promoted cell viability in fibrosarcoma, modulating iron homeostasis, and lipid peroxidation.[21] Therefore, our study is the first to reveal the functional role of FXN in modulating ovarian cancer stem-like cells viability via ferroptosis. We demonstrated that FXN downregulation reduces spheroids viability and self-renewal, increases ROS generation and TFR1 protein expression, and enhances RSL3-induced cell death. Intriguingly, TFR1, an iron-responsive element encoding protein, critical role in iron starvation response to keep iron homeostasis, and activated by iron deficiency.[45] As shown in several studies, in iron-deficient cells, TFR1 mRNA was upregulated as observed in FXN knockout mice cardiac tissues.[18] Du et al. also demonstrated that FXN knockdown upregulates TFR1, contributing to iron starvation response and ferroptosis in fibrosarcoma,[21] aligning with our findings. Taken together, we speculate that FXN deficiency disrupts iron homeostasis, triggering iron starvation response, ROS accumulation, and promoting ferroptosis in ovarian cancer stem-like cells.

ROS production is essential for ferroptosis-mediated cell death.[46] In our study, mass spectrometry analysis in Ovcar5 cells following FXN depletion revealed 104 proteins altering, with FXN tightly associated with the hydrogen peroxide catabolic process, where PRDX3 is a key protein. PRDX3, an antioxidant enzyme, protects cells from oxidative damage induced by ROS accumulation, implicated in various cellular signaling pathways and disease pathogenesis.[47] Increased mitochondrial ROS generation and disturbance of PRDX3 production can lead to oxidative stress, hypoxic microenvironments, apoptosis induction,[48] mitochondrial dysfunction,[49] and ferroptosis.[29] Studies have shown elevated PRDX3 expression in ovarian cancer tissues compared to normal tissues, predicting poor PFS and OS for ovarian cancer patients.[50] However, the previous studies are only in the preliminary stage of exploring the role of PRDX3 in ovarian cancer, and the deeper molecular mechanism remains unclear. We explored the relationship between ROS generation and PRDX3, finding that PRDX3 knockdown increased ROS accumulation and cell death. Importantly, overexpressing PRDX3 rescued ROS induction and cell viability caused by FXN deletion in spheroids, suggesting PRDX3 involvement in triggering ferroptosis induced by FXN knockdown via ROS generation.

In fact, we tried to gain deeper insights into the FXN-PRDX3 relationship. Here, we observed that PRDX3 mRNA did not significantly change following FXN downregulation, but PRDX3 protein expression changed, suggesting FXN may stabilize PRDX3 protein levels through post-translational modification. To explore the FXN pathway affecting PRDX3 expression, we treated cells with CHX. Result showed increased PRDX3 protein degradation in FXN-depletion cells. Importantly, MG132 treatment in FXN-depleted cells reduced PRDX3 degradation, suggesting FXN may protect PRDX3 from proteasome-dependent degradation, consistent with previous findings that PHB decreases PRDX3 ubiquitination and inhibits the protein degeneration in glioma stem-like cells.[33]

In conclusion, The FXN expression level was elevated in ovarian cancer and OCSLCs. FXN played a vital role by modulating PRDX3 degradation in ROS generation and ferroptosis. Therefore, the present study demonstrated that in ovarian cancer, FXN could be utilized as therapeutic target and potential diagnostic.

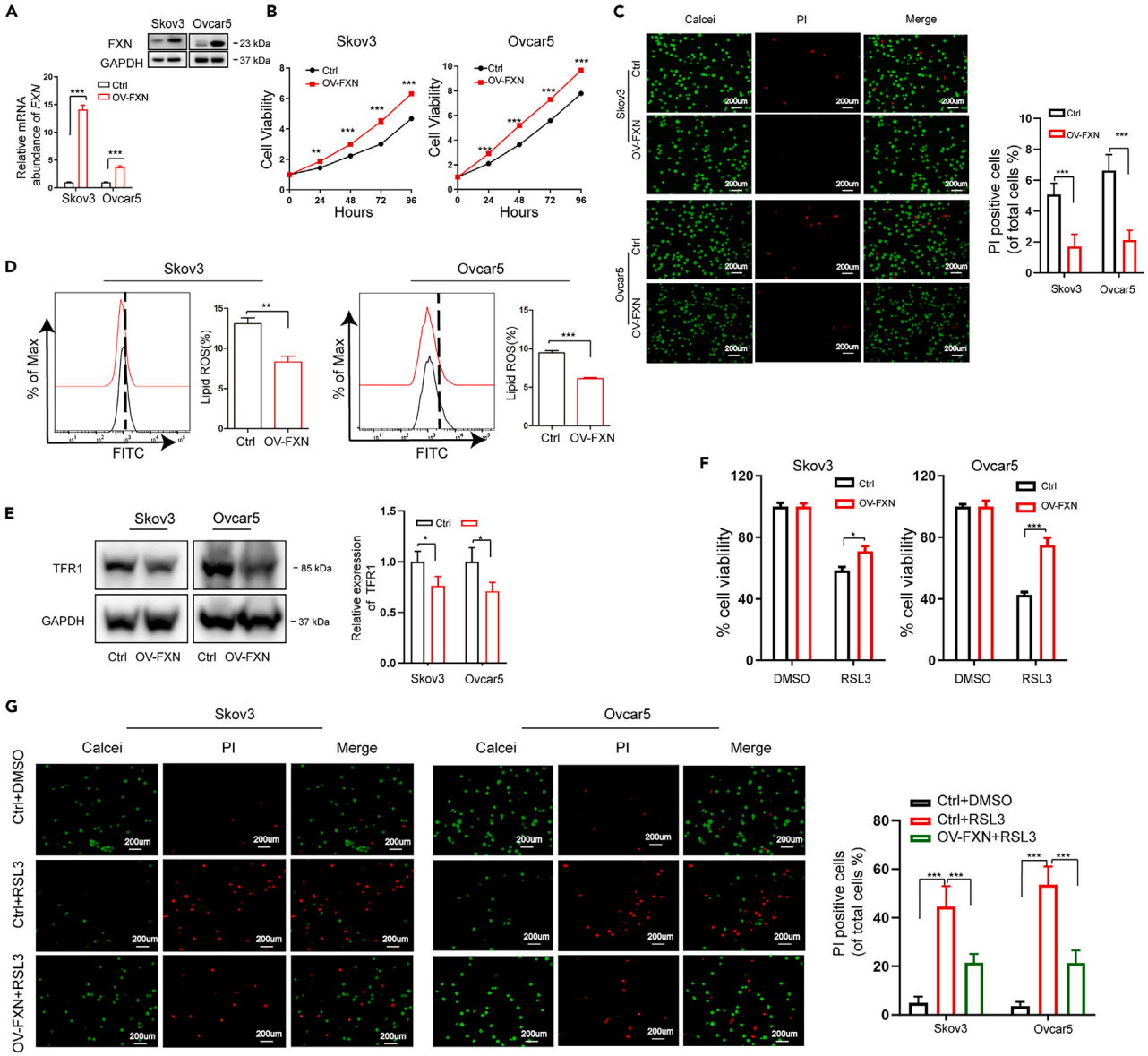

Figure 3. FXN overexpression promotes cells viability and suppresses ROS generation

(A) Quantitative real-time PCR (real-time qPCR) analysis and IB were used to verify the efficiency of FXN-overexpression in spheroids (mean ± S.E., $n = 3$, biologically independent experiments).

(B) Cell growth was performed in Ctrl and FXN-overexpression spheroids (mean ± S.E., $n = 3$, biologically independent experiments).

(C) Calcein-AM/PI staining was performed in Ctrl and FXN-overexpression spheroids (scale bar, 200 μm) (Mean ± S.E., $n = 3$, biologically independent experiments).

(D) The lipid ROS levels were measured by flow cytometry in in Ctrl and FXN-overexpression spheroids (mean ± S.E, $n = 3$, biologically independent experiments).

(E) Immunoblot illustrating the levels of TFR1 protein in the indicated spheroids (Mean ± S.E., $n = 3$, biologically independent experiments).

(F and G) Ctrl or FXN-overexpression spheroids were treated with DMSO or RSL3 for 48 h (Skov3 with 0.2μm, Ovcar5 with 10μm, respectively). Cell viability analysis is shown (F) (mean ± S.E., $n = 3$, biologically independent experiments). Calcein-AM/PI staining analysis is exhibited (G) (mean ± S.E., $n = 3$, biologically independent experiments). Statistical was assessed by unpaired t test. *$p < 0.05$, **$p < 0.01$, ***$p < 0.001$.

Limitations of the study

Ovarian cancer spheroids have been described since 2005 and have been displayed to be tumorigenic *in vivo* models that mimic the CSC phenotype.[51] This makes ovarian cancer spheroids useful tools for looking at the CSC population in ovarian cancer. However, spheroids are enriched for OCSCs, they are not exclusively, which is a limitation of this study.

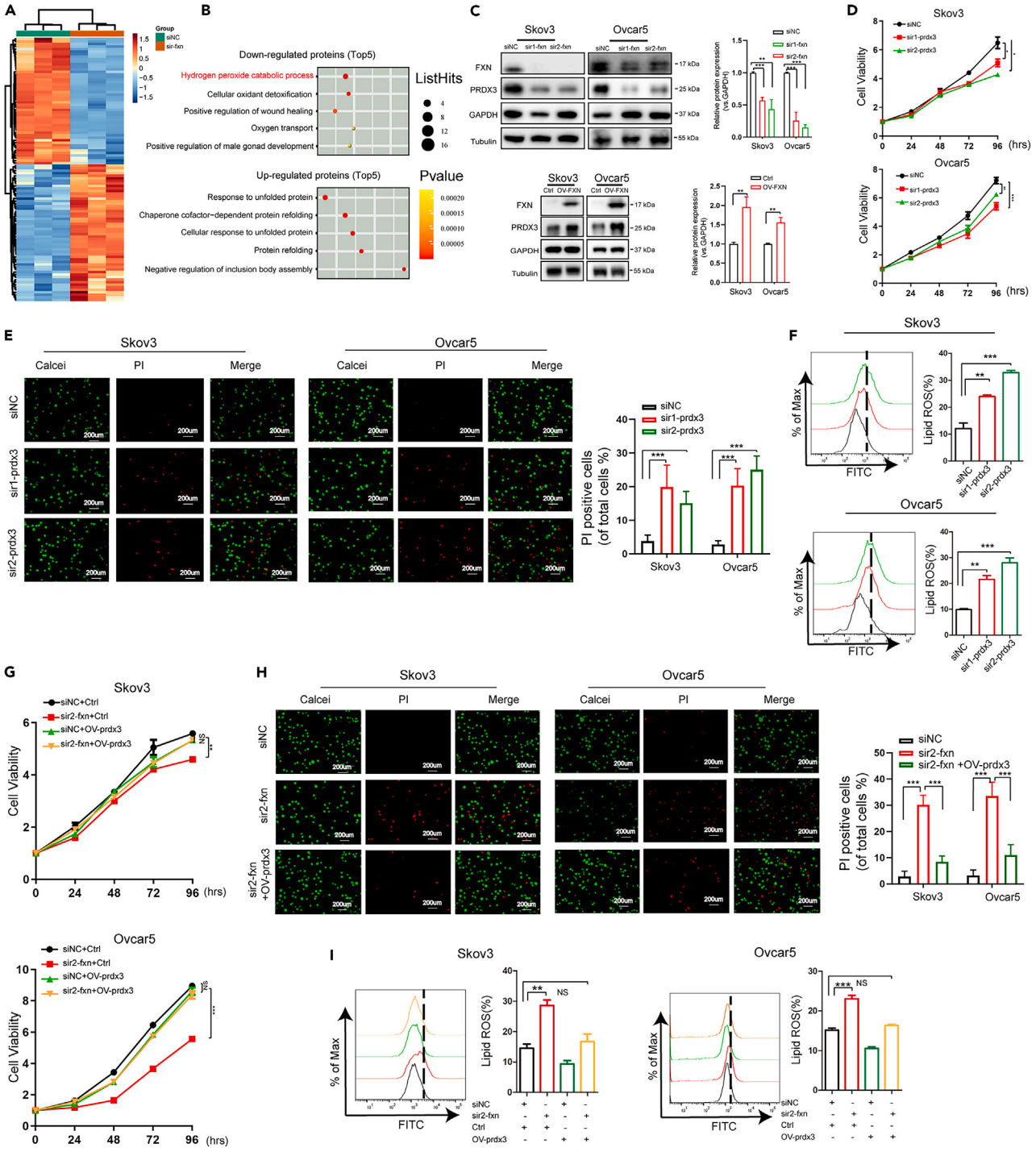

Figure 4. PRDX3 is a downstream target of FXN in ovarian cancer stem-like cells

(A) The heatmap shows relative expression levels of proteins downregulated or upregulated in the indicated cells ($p < 0.05$, FC > 1.2). It includes, respectively, 50 and 54 proteins downregulated and upregulated in FXN knockdown compared to control spheroids. Raw data were log2 transformed. A relative color scheme used the minimum and maximum values in each row to convert values to colors. Detailed information of listed in Table S1.

(B) Gene ontology (GO) terms from LC-MS/MS analysis of downregulated protein sets (top) and upregulated protein sets (bottom) in FXN KD compared to control spheroids.

(C) Immunoblot illustrating the levels of PRDX3 protein in the spheroids (mean ± S.E., $n = 3$, biologically independent experiments).

Figure 4. *Continued*

(D and E) PRDX3 knockdown (KD) spheroids were generated by siRNA system. Cell growth was assessed in Ctrl and PRDX3 KD spheroids (D) (Mean ± S.E., $n = 3$, biologically independent experiments). Calcein-AM/PI staining was performed in Ctrl and PRDX3 knockdown spheroids (E) (scale bar: 200 μm, Mean ± S.E., $n = 3$, biologically independent experiments). The lipid ROS levels, as indicated by DCFDA fluorescence, were measured by flow cytometry in PRDX3 KD and Ctrl spheroids (F) (Mean ± S.E., $n = 3$, biologically independent experiments).

(G–I) Ctrl or FXN KD spheroids were co-cultured with/without PRDX3 plasmid. Cell growth was analysis by cell viability (G) (Mean ± S.E., $n = 3$, biologically independent experiments). Calcein-AM/PI staining was performed by cell death (H) (mean ± S.E., $n = 3$, biologically independent experiments). The lipid ROS level of spheroids was detected by DCFDA fluorescence (I) (Mean ± S.E., $n = 3$, biologically independent experiments). Statistical was assessed by unpaired t test. $^{*}p < 0.05$, $^{**}p < 0.01$, $^{***}p < 0.001$, ns means no significance.

See also Table S1.

STAR★METHODS

Detailed methods are provided in the online version of this paper and include the following:

- KEY RESOURCES TABLE
- RESOURCE AVAILABILITY
  - Lead contact
  - Materials availability
  - Data and code availability
- EXPERIMENTAL MODEL AND STUDY PARTICIPANT DETAILS
  - Ethics approval and consent to participate
  - Cell lines
  - Mice
- METHOD DETAILS
  - Cell transfection
  - RNA extraction and qPCR
  - Western blot
  - Immunohistochemistry
  - The Kaplan–Meier plotter
  - Mammosphere culture and sphere-forming analysis
  - Sphere-forming analysis
  - Cell viability assay
  - Calcein-AM and PI fluorescence staining assay
  - Total lipid ROS assay
  - Proteomic analysis
  - Tumor xenograft
- QUANTIFICATION AND STATISTICAL ANALYSIS

SUPPLEMENTAL INFORMATION

Supplemental information can be found online at https://doi.org/10.1016/j.isci.2024.110506.

ACKNOWLEDGMENTS

We are grateful to Zhejiang Key Laboratory of Maternal and Infant Health for supporting our research.

Funding sources: this work was supported by the National Natural Science Foundation of China (grant number 82002728), the Zhejiang Province Medical Science and Technology Plan (grant number 2024KY1147), the Key Program of Zhejiang Province Natural Science Foundation of China (grant number LZ24H160001), the Fundamental Research Funds for the Central Universities (grant number 2023QZJH56), 4 + X Clinical Research Project of Women's Hospital, School of Medicine, Zhejiang University (grant number ZDFY2022-4X202), the National Natural Science Foundation of China (grant number 82171939), the National Natural Science Foundation of China (grant number 82103505), the Zhejiang Province Natural Science Foundation of China (grant number LQ20H160049).

AUTHOR CONTRIBUTIONS

S.X., W.L., and J.X. conceived the project. S.X. and Y.L. performed most experiments. W.F. and S.Y. performed the tumor xenograft mouse experiments. J.Q. conducted statistical analyses. S.X. wrote the original draft with input from all authors. J.X. revised the paper. W.L. and J.X. supervised the project.

DECLARATION OF INTERESTS

Authors declare that they have no conflict of interests.

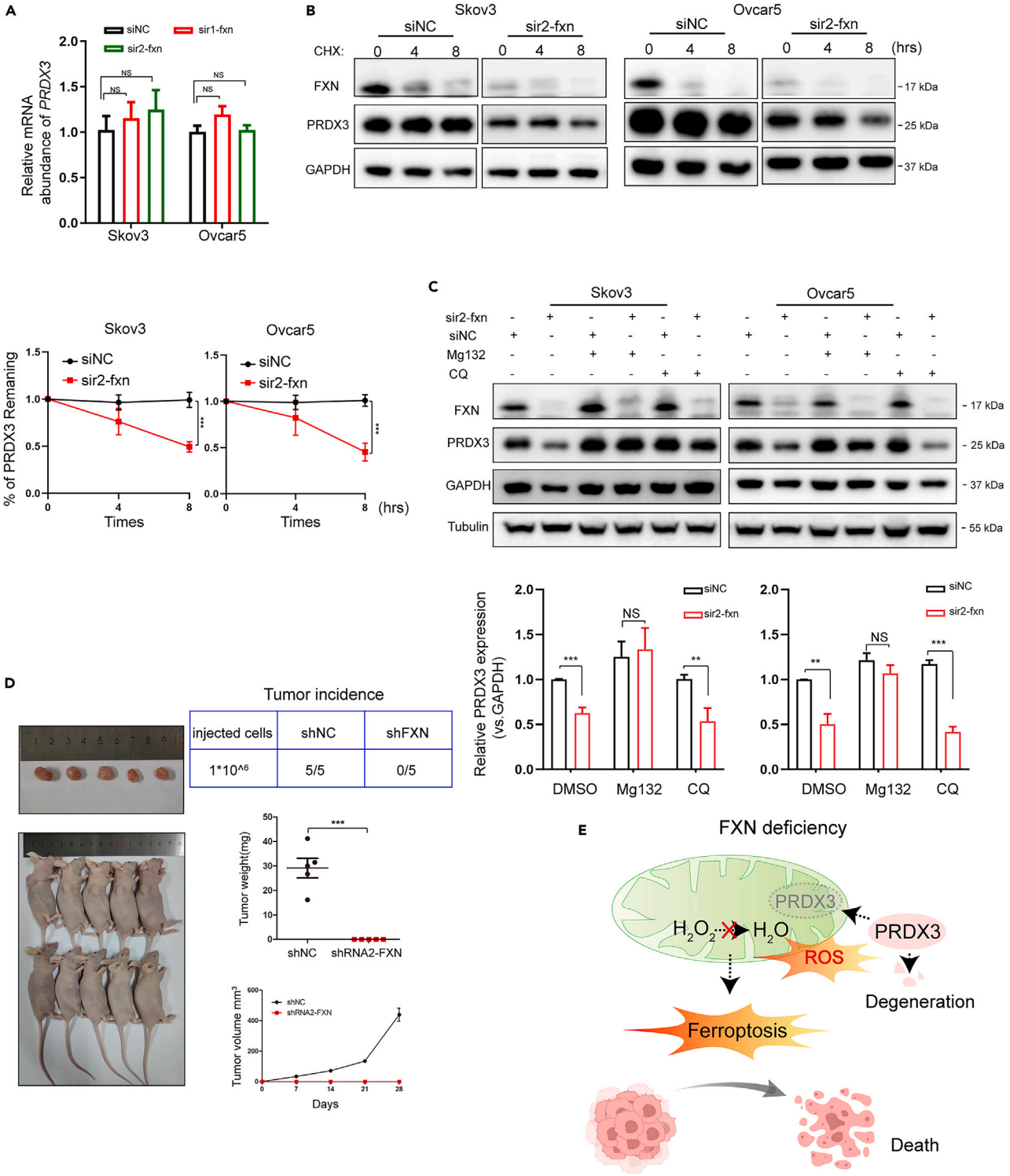

Figure 5. FXN stabilizes PRDX3 by inhibiting its proteasome degradation

(A) Real-time qPCR analysis of mRNA levels of indicated genes in Ctrl and FXN KD spheroids (mean ± S.E., *n* = 3, biologically independent experiments).

(B) IB showing the CHX (50 μg/mL) chase analysis of PRDX3 protein degradation at indicated time points in spheroids with or without FXN KD (mean ± S.E., *n* = 3, biologically independent experiments).

(C) IB showing the levels of PRDX3 and FXN in FXN KD spheroids treated with MG132 (5 μM) or CQ (5 μM) for 12 h (mean ± S.E., *n* = 3, biologically independent experiments).

Figure 5. *Continued*

(D) Skov3 cells were transfected with Ctrl or shRNA-FXN for 48 h, maintained in spheroid culture conditions for 7 days, and then spheroids were collected and trypsin digested into single cells. After counting, 1×10^6 live cells were injected subcutaneously into BALB/c Nude mice ($n = 5$ in each group). All mice were sacrificed at week 4 and subcutaneous tumors are shown (left upper panel). The tumor incidence was evaluated (right upper panel). Tumor volume was calculated (middle panel) and diameters were measured at a regular interval of 1 week for up to 4 weeks (bottom right panel). The level of significance is indicated by $^{**}p < 0.01$, $^{***}p < 0.001$, ns means no significance.

(E) Model of FXN-PRDX3 regulation axis. In OCSLCs, Loss of FXN increases PRDX3 degradation, elevates ROS levels, and subsequently induces OCSLCs death.

Received: March 5, 2024
Revised: June 14, 2024
Accepted: July 11, 2024
Published: July 14, 2024

REFERENCES

1. Siegel, R.L., Miller, K.D., Wagle, N.S., and Jemal, A. (2023). Cancer statistics, 2023. CA. Cancer J. Clin. *73*, 17–48. https://doi.org/10.3322/caac.21763.
2. Wang, Z., Yan, Y., Lou, Y., Huang, X., Liu, L., Weng, Z., Cui, Y., Wu, X., Cai, H., Chen, X., and Ji, Y. (2023). Diallyl trisulfide alleviates chemotherapy sensitivity of ovarian cancer via the AMPK/SIRT1/PGC1α pathway. Cancer Sci. *114*, 357–369. https://doi.org/10.1111/cas.15627.
3. Buechel, M., Herzog, T.J., Westin, S.N., Coleman, R.L., Monk, B.J., and Moore, K.N. (2019). Treatment of patients with recurrent epithelial ovarian cancer for whom platinum is still an option. Ann. Oncol. *30*, 721–732. https://doi.org/10.1093/annonc/mdz104.
4. Mihanfar, A., Aghazadeh Attari, J., Mohebbi, I., Majidinia, M., Kaviani, M., Yousefi, M., and Yousefi, B. (2019). Ovarian cancer stem cell: A potential therapeutic target for overcoming multidrug resistance. J. Cell. Physiol. *234*, 3238–3253. https://doi.org/10.1002/jcp.26768.
5. Lheureux, S., Gourley, C., Vergote, I., and Oza, A.M. (2019). Epithelial ovarian cancer. Lancet *393*, 1240–1253. https://doi.org/10.1016/S0140-6736(18)32552-2.
6. Vasan, N., Baselga, J., and Hyman, D.M. (2019). A view on drug resistance in cancer. Nature *575*, 299–309. https://doi.org/10.1038/s41586-019-1730-1.
7. Tossetta, G., Fantone, S., Goteri, G., Giannubilo, S.R., Ciavattini, A., and Marzioni, D. (2023). The Role of NQO1 in Ovarian Cancer. Int. J. Mol. Sci. *24*, 7839. https://doi.org/10.3390/ijms24097839.
8. Fantone, S., Piani, F., Olivieri, F., Rippo, M.R., Sirico, A., Di Simone, N., Marzioni, D., and Tossetta, G. (2024). Role of SLC7A11/xCT in Ovarian Cancer. Int. J. Mol. Sci. *25*, 587. https://doi.org/10.3390/ijms25010587.
9. Taylor, W.R., Fedorka, S.R., Gad, I., Shah, R., Alqahtani, H.D., Koranne, R., Kuganesan, N., Dlamini, S., Rogers, T., Al-Hamashi, A., et al. (2019). Small-Molecule Ferroptotic Agents with Potential to Selectively Target Cancer Stem Cells. Sci. Rep. *9*, 5926. https://doi.org/10.1038/s41598-019-42251-5.
10. Liu, C.C., Li, H.H., Lin, J.H., Chiang, M.C., Hsu, T.W., Li, A.F., Yen, D.H., Hsu, H.S., and Hung, S.C. (2021). Esophageal Cancer Stem-like Cells Resist Ferroptosis-Induced Cell Death by Active Hsp27-GPX4 Pathway. Biomolecules *12*, 48. https://doi.org/10.3390/biom12010048.
11. Brown, J.R., Chan, D.K., Shank, J.J., Griffith, K.A., Fan, H., Szulawski, R., Yang, K., Reynolds, R.K., Johnston, C., McLean, K., et al. (2020). Phase II clinical trial of metformin as a cancer stem cell-targeting agent in ovarian cancer. JCI Insight *5*, e133247. https://doi.org/10.1172/jci.insight.133247.
12. Du, F.Y., Zhou, Q.F., Sun, W.J., and Chen, G.L. (2019). Targeting cancer stem cells in drug discovery: Current state and future perspectives. World J. Stem Cells *11*, 398–420. https://doi.org/10.4252/wjsc.v11.i7.398.
13. Elgendy, S.M., Alyammahi, S.K., Alhamad, D.W., Abdin, S.M., and Omar, H.A. (2020). Ferroptosis: An emerging approach for targeting cancer stem cells and drug resistance. Crit. Rev. Oncol. Hematol. *155*, 103095. https://doi.org/10.1016/j.critrevonc.2020.103095.
14. Wang, Y., Zhao, G., Condello, S., Huang, H., Cardenas, H., Tanner, E.J., Wei, J., Ji, Y., Li, J., Tan, Y., et al. (2021). Frizzled-7 Identifies Platinum-Tolerant Ovarian Cancer Cells Susceptible to Ferroptosis. Cancer Res. *81*, 384–399. https://doi.org/10.1158/0008-5472.CAN-20-1488.
15. Huang, Y., Lin, J., Xiong, Y., Chen, J., Du, X., Liu, Q., and Liu, T. (2020). Superparamagnetic Iron Oxide Nanoparticles Induce Ferroptosis of Human Ovarian Cancer Stem Cells by Weakening Cellular Autophagy. J. Biomed. Nanotechnol. *16*, 1612–1622. https://doi.org/10.1166/jbn.2020.2991.
16. Xuan, Y., Wang, H., Yung, M.M., Chen, F., Chan, W.S., Chan, Y.S., Tsui, S.K., Ngan, H.Y., Chan, K.K., and Chan, D.W. (2022). SCD1/FADS2 fatty acid desaturases equipoise lipid metabolic activity and redox-driven ferroptosis in ascites-derived ovarian cancer cells. Theranostics *12*, 3534–3552. https://doi.org/10.7150/thno.70194.
17. Koutnikova, H., Campuzano, V., Foury, F., Dolle, P., Cazzalini, O., and Koenig, M. (1997). Studies of human, mouse and yeast homologues indicate a mitochondrial function for frataxin. Nat. Genet. *16*, 345–351. https://doi.org/10.1038/ng0897-345.
18. Huang, M.L., Becker, E.M., Whitnall, M., Suryo Rahmanto, Y., Ponka, P., and Richardson, D.R. (2009). Elucidation of the mechanism of mitochondrial iron loading in Friedreich's ataxia by analysis of a mouse mutant. Proc. Natl. Acad. Sci. USA *106*, 16381–16386. https://doi.org/10.1073/pnas.0906784106.
19. Gomes, C.M., and Santos, R. (2013). Neurodegeneration in Friedreich's ataxia: from defective frataxin to oxidative stress. Oxid. Med. Cell. Longev. *2013*, 487534. https://doi.org/10.1155/2013/487534.
20. Turchi, R., Tortolici, F., Guidobaldi, G., Iacovelli, F., Falconi, M., Rufini, S., Faraonio, R., Casagrande, V., Federici, M., De Angelis, L., et al. (2020). Frataxin deficiency induces lipid accumulation and affects thermogenesis in brown adipose tissue. Cell Death Dis. *11*, 51. https://doi.org/10.1038/s41419-020-2253-2.
21. Du, J., Zhou, Y., Li, Y., Xia, J., Chen, Y., Chen, S., Wang, X., Sun, W., Wang, T., Ren, X., et al. (2020). Identification of Frataxin as a regulator of ferroptosis. Redox Biol. *32*, 101483. https://doi.org/10.1016/j.redox.2020.101483.
22. Paupe, V., Dassa, E.P., Goncalves, S., Auchere, F., Lonn, M., Holmgren, A., and Rustin, P. (2009). Impaired nuclear Nrf2 translocation undermines the oxidative stress response in Friedreich ataxia. PLoS One *4*, e4253. https://doi.org/10.1371/journal.pone.0004253.
23. Shi, M.F., Jiao, J., Lu, W.G., Ye, F., Ma, D., Dong, Q.G., and Xie, X. (2010). Identification of cancer stem cell-like cells from human epithelial ovarian carcinoma cell line. Cell. Mol. Life Sci. *67*, 3915–3925. https://doi.org/10.1007/s00018-010-0420-9.
24. Xu, S., Yue, Y., Zhang, S., Zhou, C., Cheng, X., Xie, X., Wang, X., and Lu, W. (2018). STON2 negatively modulates stem-like properties in ovarian cancer cells via DNMT1/MUC1 pathway. J. Exp. Clin. Cancer Res. *37*, 305. https://doi.org/10.1186/s13046-018-0977-y.
25. Ghazizadeh, M. (2003). Cisplatin may induce frataxin expression. J. Nippon Med. Sch. *70*, 367–371. https://doi.org/10.1272/jnms.70.367.
26. Thierbach, R., Schulz, T.J., Isken, F., Voigt, A., Mietzner, B., Drewes, G., von Kleist-Retzow, J.C., Wiesner, R.J., Magnuson, M.A., Puccio, H., et al. (2005). Targeted disruption of hepatic frataxin expression causes impaired mitochondrial function, decreased life span and tumor growth in mice. Hum. Mol. Genet. *14*, 3857–3864. https://doi.org/10.1093/hmg/ddi410.
27. Palomo, G.M., Cerrato, T., Gargini, R., and Diaz-Nido, J. (2011). Silencing of frataxin gene expression triggers p53-dependent apoptosis in human neuron-like cells. Hum. Mol. Genet. *20*, 2807–2822. https://doi.org/10.1093/hmg/ddr187.
28. Moreno-Lorite, J., Perez-Luz, S., Katsu-Jimenez, Y., Oberdoerfer, D., and Diaz-Nido, J. (2021). DNA repair pathways are altered in neural cell models of frataxin deficiency. Mol. Cell. Neurosci. *111*, 103587. https://doi.org/10.1016/j.mcn.2020.103587.

29. Cui, S., Ghai, A., Deng, Y., Li, S., Zhang, R., Egbulefu, C., Liang, G., Achilefu, S., and Ye, J. (2023). Identification of hyperoxidized PRDX3 as a ferroptosis marker reveals ferroptotic damage in chronic liver diseases. Mol. Cell *83*, 3931–3939.e5. https://doi.org/10.1016/j.molcel.2023.09.025.
30. Elumalai, S., Karunakaran, U., Moon, J.S., and Won, K.C. (2020). High glucose-induced PRDX3 acetylation contributes to glucotoxicity in pancreatic beta-cells: Prevention by Teneligliptin. Free Radic. Biol. Med. *160*, 618–629. https://doi.org/10.1016/j.freeradbiomed.2020.07.030.
31. Lynch, J., Wang, Y., Li, Y., Kavdia, K., Fukuda, Y., Ranjit, S., Robinson, C.G., Grace, C.R., Xia, Y., Peng, J., and Schuetz, J.D. (2023). A PPIX-binding probe facilitates discovery of PPIX-induced cell death modulation by peroxiredoxin. Commun. Biol. *6*, 673. https://doi.org/10.1038/s42003-023-05024-5.
32. Wang, G., Li, X., Li, N., Wang, X., He, S., Li, W., Fan, W., Li, R., Liu, J., and Hou, S. (2022). Icariin alleviates uveitis by targeting peroxiredoxin 3 to modulate retinal microglia M1/M2 phenotypic polarization. Redox Biol. *52*, 102297. https://doi.org/10.1016/j.redox.2022.102297.
33. Huang, H., Zhang, S., Li, Y., Liu, Z., Mi, L., Cai, Y., Wang, X., Chen, L., Ran, H., Xiao, D., et al. (2021). Suppression of mitochondrial ROS by prohibitin drives glioblastoma progression and therapeutic resistance. Nat. Commun. *12*, 3720. https://doi.org/10.1038/s41467-021-24108-6.
34. Padma, V.V. (2015). An overview of targeted cancer therapy. Biomedicine *5*, 19. https://doi.org/10.7603/s40681-015-0019-4.
35. Zhang, H., and Chen, J. (2018). Current status and future directions of cancer immunotherapy. J. Cancer *9*, 1773–1781. https://doi.org/10.7150/jca.24577.
36. Mansoori, B., Mohammadi, A., Davudian, S., Shirjang, S., and Baradaran, B. (2017). The Different Mechanisms of Cancer Drug Resistance: A Brief Review. Adv. Pharm. Bull. *7*, 339–348. https://doi.org/10.15171/apb.2017.041.
37. Bai, X., Ni, J., Beretov, J., Graham, P., and Li, Y. (2018). Cancer stem cell in breast cancer therapeutic resistance. Cancer Treat Rev. *69*, 152–163. https://doi.org/10.1016/j.ctrv.2018.07.004.
38. Shakhova, O., and Sommer, L. (2013). Testing the cancer stem cell hypothesis in melanoma: the clinics will tell. Cancer Lett. *338*, 74–81. https://doi.org/10.1016/j.canlet.2012.10.009.
39. Liu, Y.C., Yeh, C.T., and Lin, K.H. (2020). Cancer Stem Cell Functions in Hepatocellular Carcinoma and Comprehensive Therapeutic Strategies. Cells *9*, 1331. https://doi.org/10.3390/cells9061331.
40. Yang, L., Shi, P., Zhao, G., Xu, J., Peng, W., Zhang, J., Zhang, G., Wang, X., Dong, Z., Chen, F., and Cui, H. (2020). Targeting cancer stem cell pathways for cancer therapy. Signal Transduct. Target. Ther. *5*, 8. https://doi.org/10.1038/s41392-020-0110-5.
41. Tesfay, L., Paul, B.T., Konstorum, A., Deng, Z., Cox, A.O., Lee, J., Furdui, C.M., Hegde, P., Torti, F.M., and Torti, S.V. (2019). Stearoyl-CoA Desaturase 1 Protects Ovarian Cancer Cells from Ferroptotic Cell Death. Cancer Res. *79*, 5355–5366. https://doi.org/10.1158/0008-5472.CAN-19-0369.
42. Basuli, D., Tesfay, L., Deng, Z., Paul, B., Yamamoto, Y., Ning, G., Xian, W., McKeon, F., Lynch, M., Crum, C.P., et al. (2017). Iron addiction: a novel therapeutic target in ovarian cancer. Oncogene *36*, 4089–4099. https://doi.org/10.1038/onc.2017.11.
43. Lane, D.J., Merlot, A.M., Huang, M.L., Bae, D.H., Jansson, P.J., Sahni, S., Kalinowski, D.S., and Richardson, D.R. (2015). Cellular iron uptake, trafficking and metabolism: Key molecules and mechanisms and their roles in disease. Biochim. Biophys. Acta *1853*, 1130–1144. https://doi.org/10.1016/j.bbamcr.2015.01.021.
44. Gao, G., and Chang, Y.Z. (2014). Mitochondrial ferritin in the regulation of brain iron homeostasis and neurodegenerative diseases. Front. Pharmacol. *5*, 19. https://doi.org/10.3389/fphar.2014.00019.
45. Bogdan, A.R., Miyazawa, M., Hashimoto, K., and Tsuji, Y. (2016). Regulators of Iron Homeostasis: New Players in Metabolism, Cell Death, and Disease. Trends Biochem. Sci. *41*, 274–286. https://doi.org/10.1016/j.tibs.2015.11.012.
46. Stockwell, B.R., Friedmann Angeli, J.P., Bayir, H., Bush, A.I., Conrad, M., Dixon, S.J., Fulda, S., Gascon, S., Hatzios, S.K., Kagan, V.E., et al. (2017). Ferroptosis: A Regulated Cell Death Nexus Linking Metabolism, Redox Biology, and Disease. Cell *171*, 273–285. https://doi.org/10.1016/j.cell.2017.09.021.
47. Ray, P.D., Huang, B.W., and Tsuji, Y. (2012). Reactive oxygen species (ROS) homeostasis and redox regulation in cellular signaling. Cell. Signal. *24*, 981–990. https://doi.org/10.1016/j.cellsig.2012.01.008.
48. Wang, Z., Sun, R., Wang, G., Chen, Z., Li, Y., Zhao, Y., Liu, D., Zhao, H., Zhang, F., Yao, J., and Tian, X. (2020). SIRT3-mediated deacetylation of PRDX3 alleviates mitochondrial oxidative damage and apoptosis induced by intestinal ischemia/reperfusion injury. Redox Biol. *28*, 101343. https://doi.org/10.1016/j.redox.2019.101343.
49. Zhang, S., Wu, X., Wang, J., Shi, Y., Hu, Q., Cui, W., Bai, H., Zhou, J., Du, Y., Han, L., et al. (2022). Adiponectin/AdiopR1 signaling prevents mitochondrial dysfunction and oxidative injury after traumatic brain injury in a SIRT3 dependent manner. Redox Biol. *54*, 102390. https://doi.org/10.1016/j.redox.2022.102390.
50. Li, S., Hu, X., Ye, M., and Zhu, X. (2018). The prognostic values of the peroxiredoxins family in ovarian cancer. Biosci. Rep. *38*, BSR20180667. https://doi.org/10.1042/BSR20180667.
51. Bapat, S.A., Mali, A.M., Koppikar, C.B., and Kurrey, N.K. (2005). Stem and progenitor-like cells contribute to the aggressive behavior of human epithelial ovarian cancer. Cancer Res. *65*, 3025–3029. https://doi.org/10.1158/0008-5472.CAN-04-3931.

STAR★METHODS

KEY RESOURCES TABLE

REAGENT or RESOURCE	SOURCE	IDENTIFIER
Antibodies		
Rabbit anti-FXN	Proteintech	Cat # 14147-1-AP; RRID: AB_2231876
Rabbit anti-GAPDH	Abcam	Cat #ab9485; RRID: AB_307275
Rabbit anti-PRDX3	Abclonal	Cat #A2398; RRID: AB_2863001
Rabbit anti-Nanog	Abcam	Cat #109250; RRID: AB_10863442
Rabbit anti-TFR1	Abclonal	Cat #A5865; RRID: AB_2766615
Mouse anti-P53	Abclonal	Cat #A10610; RRID: AB_2758147
Mouse anti-Tubulin	Proteintech	Cat #66031-1-Ig; RRID:AB_11042766
Goat anti-mouse IgG (H+L)	Thermo Fisher Scientific	Cat #31430; RRID:AB_228307
Goat anti-rabbit IgG (H+L)	Thermo Fisher Scientific	Cat #31460; RRID: AB_228341
Bacterial and virus strains		
Lentivirus-expressing GV112 - shCtrl	This paper	N/A
Lentivirus-expressing GV112 - sh-FXN2	This paper	N/A
Biological samples		
Formed tumors in BALB/c Nude mice	This paper	N/A
Ovarian cancer tissue	This paper	N/A
Paraffin-embedded ovarian cancer specimens	This paper	N/A
Chemicals, peptides, and recombinant proteins		
TRIzol reagent	Thermo Fisher Scientific	Cat# 15596018
RIPA buffer	Thermo Fisher Scientific	Cat# 89900
Proteinase inhibitor cocktail	Thermo Fisher Scientific	Cat# 7843
Puromycin	Thermo Fisher Scientific	Cat# A1113803
Erastin	MCE	Cat# HY-15763
RSL3	MCE	Cat# HY-100218A
CM-H2DCFDA	Sigma-Aldrich	Cat #287810
CCK reagent	Dojindo	Cat #CK04
Critical commercial assays		
PrimeScript™ RT reagent Kit with gDNA Eraser kit	Takara	Cat# RR047A
SYBR® Premix Ex Taq™ II (Tli RNaseH Plus)	Takara	Cat# RR820A
SuperSignal® West Pico Chemiluminescent Substrate	Thermo Fisher Scientific	Cat# 34578
Calcein-AM/PI kit	Yeasen	Cat# 40747ES76
Deposited data		
Proteomics	This study	iPROX: IPX0007691000
Experimental models: Cell lines		
Skov3	ATCC	Cat# HTB-77
Ovcar5	Lab stock	N/A
Experimental models: Organisms/strains		
BALB/c Nude mice	Hangsi biological	N/A

(*Continued on next page*)

Continued

REAGENT or RESOURCE	SOURCE	IDENTIFIER
Oligonucleotides		
shRNA targeting sequence: shFXN2: GAACCTATGTGATCAACAA	This paper	N/A
SiRNA targeting sequences, see Table S3	This paper	N/A
Primers used for qRT-PCR, see Table S4	This paper	N/A
Primers used for plasmid construction, see Table S4	This paper	N/A
Recombinant DNA		
LT-Flag vector	This paper	N/A
LT-Flag FXN	This paper	N/A
Software and algorithms		
GraphPad Prism 8.0	GraphPad	https://www.graphpad.com/
FlowJo X software	Ashland	https://www.flowjo.com/
Image Lab 5.2	BIO-RAD	https://www.bio-rad.com/zh-cn/product/image-lab-software?ID=KRE6P5E8Z
ImageJ software	National Institutes of Health	https://ImageJ.en.softonic.com/mac
Other		
Lipofectamine™ RNAiMAX	Thermo Fisher Scientific	Cat# 13778150
Opti-MEMTM I medium	Thermo Fisher Scientific	Cat# 31985088
DMEM/F12 medium	BI	Cat# 06-1170-87-1A
B27 additive	Life Technologies	Cat# 17504044
Insulin	Sigma-Aldrich	Cat# 91077C
Human EGF Recombinant Protein	Thermo Fisher Scientific	Cat# AF-100-15-1MG
Human FGF-basic (FGF-2/bFGF)	Thermo Fisher Scientific	Cat# AF-100-18B-1MG

RESOURCE AVAILABILITY

Lead contact

Further information and requests for resources and reagents should be directed to and will be fulfilled by the lead contact, Junfen Xu (xjfzu@zju.edu.cn).

Materials availability

This study did not generate new unique reagents. All the cell lines used in this manuscript will be made available upon request.

Data and code availability

- Date: The novel proteomic data generated in this paper were deposited in the Integrated Proteome Resources (iPROX), an integrated proteome resources center in China, and are publicly available as of the date of publication. Accession number is listed in the key resources table.
- Code: This paper does not report original code.
- All other requests: Any additional information required to reanalyze the data reported will be shared by the lead contact upon request.

EXPERIMENTAL MODEL AND STUDY PARTICIPANT DETAILS

Ethics approval and consent to participate

All animal treatments were performed in accordance with Animal Research Reporting *In Vivo* Experiments (ARRIVE) guidelines and were approved by the ethics committee of Women's Hospital of Zhejiang University School of Medicine (approval no. AE 20230002). For IHC staining, 178 tumor samples were obtained from ovarian cancer patients who underwent tumor resection surgery in the Women's Hospital of Zhejiang University School of Medicine from January 2002 to December 2009. The clinical features of these patients are summarized in Table S2. This study was approved by the ethics committee of Women's Hospital of Zhejiang University School of Medicine (approval no.IRB-20240049-R). All patients in this study provided their informed consent.

Cell lines

Skov3 cells were grown in Dulbecco's Modified Eagle Medium (#C12430500BT, Gibco, Waltham, MA, USA), while Ovcar5 cells were maintained in RPMI 1640 medium (#C22400500BT, Gibco, Waltham, MA, USA), supplemented with 10% fetal bovine serum (#16140071, Gibco, Waltham, MA, USA) and 100 units/ml penicillin, cultured in a 37°C incubator with 5% CO2 and detached using trypsin/EDTA solution.

Mice

A total of ten female 4-6-week-old BALB/c nude mice (14-16g, Strain NO. SM-014) were purchased from the Chinese Academy of Medical Sciences (Beijing, China). The mice were housed under specific-pathogen-free conditions at (18-23°C) and humidity (40-60%) with free access to standard sterile food and water and a 12-h light/dark cycle.

METHOD DETAILS

Cell transfection

Human FXN genes were inserted in pcDNA3.1 (+) vector and the empty vector was used as the negative control. The short-hairpin RNAs (shRNAs) for FXN were cloned into hU6-MCSCMV-puromycin lentivirus expression vectors between the AgeI and EcoRI sites. Control and On-target siRNA pools for FXN and PRDX3, were purchased from Genepharma (Shanghai, China). Targets used for silencing gene expression are listed in Table S3. Cells were seeded in growth media at 2×10^5 cells per 6-well plate the day prior to transfection. Then cells were transfected with 50 nM siRNA or 2 μg vector DNA, using Lipofectamine 3000 transfection reagents following the manufacturer's instruction (ThermoFisher, Waltham, MA, USA). Primers used for plasmid construction of FXN based on pcDNA3.1 vector (Sigma-Aldrich) are listed in Table S4.

RNA extraction and qPCR

Total RNA was extracted by an RNA extraction kit (TaKaRa, Dalian, China), and reverse-transcribed into cDNA through reverse transcription cDNA kit (TAKAR, Dalian, China). Then the PCR reactions were performed in biosystems 7900HT fast real-time PCR system (Life Technologies, Carlsbad, California, USA) with SYBR® Premix Ex Taq™ (TaKaRa, Dalian, China). Finally, the relative mRNA expression was calculated using the 2-ΔΔCt method and normalized to GAPDH expression. Primers used for qRT-PCR are listed in Table S4.

Western blot

Cells were collected and lysed with radioimmunoprecipitation assay (RIPA) buffer supplemented with cocktail. Protein concentrations loaded and separated on a 12% sodium dodecyl sulfate polyacrylamide gel and electrotransferred onto 0.22-μm polyvinylidene fluoride (PVDF) membranes. The membranes were blocked with TBST buffer (20 mM Trisbuffered saline and 0.5% Tween 20) containing 5% bovine serum albumin for 1 hour at room temperature followed by corresponding primary antibodies overnight at 4°C. After washing with TBST buffer thrice, secondary antibodies were used at 1:10000 dilutions for 1 h at room temperature. Protein detection was performed using an enhanced chemiluminescence (ECL) kit (ThermoFisher, Waltham, MA, USA) and photographed by an Image quant LAS400 mini (GE Healthcare, Munich, Germany).

Immunohistochemistry

With the permission of the patients and the ethical committee of the Women's Hospital, School of Medicine, Zhejiang University, 178 formalin-fixed and paraffin-embedded ovarian cancer specimens were immunostained with FXN antibody (#14147-1-AP). Following by visualized using 3,30-diaminobenzidine chromogen (Zhongshan Golden Bridge). Briefly, presence or absence of FXN staining was scored by five microscope fields, each has been assessed both the intensity of the staining and the percentage of positively stained cells. For the intensity, a score of 1–4 (corresponding to negative, weak, moderate, or strong staining) was recorded (Figure S1D) and the percentage of positively stained cells at each intensity, a score of 1-4 (according to 0∼25%, 25∼50%, 50∼75%, 75∼100%) was estimated. The score for each microscopic field was obtained by multiplying the two parts of score. Finally, adding the scores of the five microscopic fields. The sum from 1 to 42 was assigned as "low expression", from 43 to 80 was assigned as "high expression. In addition, since 20 patients failed to re-contact, only the remaining 158 patients were used for the calculation of progression-free survival (PFS) and overall survival. See also Table S2.

The Kaplan–Meier plotter

The Kaplan-Meier plotter (http://kmplot.com/analysis/) was used to investigate the correlation between FXN mRNA levels and PFS of 1436 ovarian cancer patients on Affymetrix id 230234_at. To explore the prognostic significance of a particular gene, the ovarian cancer samples were divided into "low" and "high" expression. Subsequently, FXN was put into the database to acquire PFS Kaplan-Meier plotter. Hazard ratio (HR), 95%, log rank P and confidence intervals (95% CI) were calculated and presented on the webpage (http://kmplot.com/analysis/index.php?p=service).

Mammosphere culture and sphere-forming analysis

This experiment was referred to the previous work (Xu et al., 2018). Briefly, 5×10^4 cells per ultra-low attachment 6-well were cultured in serum-free medium (SFM) composed of Dulbecco's modified Eagle's medium (DMEM)/F12 (BI, Kibbutz Beit-Haemek, Israel), 10μL/mL B27 additive

(Life Technologies,Carlsbad, California, USA), 1mg/mL insulin (Sigma-Aldrich,Burlington, MA, USA),10ng/mL basic fibroblast growth factor and 20ng/mL epidermal growth factor (Pepro-Tech, Rocky Hill, USA) ,and maintained at 37°C in 5% CO2 for 7 days. Fresh medium was added after every two or three days.

Sphere-forming analysis

Skov3 or Ovcar5 cells were seeded in growth media at 2×10^5 cells per 6-well plate, next day cells were transfected with control and on-target siRNA pools of FXN for 24h. then we collected cells and seeded 400 cells/well. into ultra-low attachment 96-well culture plates (Corning, New York, USA) and cultured with SFM for 7 days. After then, spheroids > 50 μm were observed and counted under the microscope.

Cell viability assay

Spheroids were collected and trypsin digested into single cells. After counting, 3×10^3 or 5×10^3 live cells were seeded into 96-well culture plates treated with compounds or transfected with over-expression plasmid/ siRNA as indicated in legends. Subsequently, CCK reagent (#CK04, Dojindo, Kyushu Island, Japan) was added to each well, followed by incubation for 2 hours at 37°C in 5% CO2. Absorbance at 450 nm was measured using a microplate reader (Thermo VARIOSKAN FLASH, Waltham, MA, USA).

Calcein-AM and PI fluorescence staining assay

The number of living and dead cells was counted using the Calcein-AM/PI double staining (#40747ES76, Yeasen, China) test for cell death. Briefly, cells were seeded in 6-well ultra-low attachment (5 × 104/ well) with serum-free medium for 7 days. Then spheroids were collected and trypsin digested into single cells. After counting, cells were seeded in 12-well at 5 × 104 cells per well 37°C and 5% CO2. After 24 h, cells were treated with compounds or transfected with over-expression plasmid/siRNA as indicated in legends. After another 48 h, cells were incubated for 30 min at 37°C in the dark with Calcein-AM test solution (2μM) and PI test solution (4.5 μM). Then photographed by a fluorescence microscope (DM4000B, Lecia) and calculated the ratio of dying cells to total cells using mage J.

Total lipid ROS assay

Spheroids were collected and trypsin digested into single cells. After counting, 2×10^5 cells per 6-well plate, next day cells were transfected with control and on-target siRNA pools of FXN for 24h or treated as indicated in legends for the times indicated. Cells collected and remained in the dark with CM-H2DCFDA (10μM) for 30 min at 37°C followed by trypsinization and three wash with 1X PBS (Gibco) and measured by a flow cytometry (BD FACSVerse, BD Biosciences, San Jose, CA, USA) in combination with FlowJo X software (FlowJo LLC, Ashland, OR, USA).

Proteomic analysis

Ovcar5 spheroids cells were collected and trypsin digested into single cells, then seeded into 10cm culture dish and transfected with sirFXN or siNC. transfected with sirFXN or siNC (three biological replicates in each group) were underwent proteomics analyses via LC-MS/MS. 50 μg of protein from each sample were adjusted to 300 μl 8M urea on ice, followed by alkylation for 20 min with 10 mM iodoacetamide in the dark. Proteins were digested to peptides with trypsin (Promega Madison, Wisconsin, USA) overnight at 37°C. The following day, the peptides were desalted on C18 cartridges (Sigma, Burlington, MA, USA) and centrifuged for 1 min at 55 g, followed by resuspending in 200 μl 0.1% trifluoroacetic acid. LC-MS/MS analysis was performed on a Finnigan LTQ VELOS MS (ThermoFisher, Waltham, MA, USA). The proteomics statistical analyses were performed using DeCyder differential analysis software (GE Healthcare, Munich, Germany).

Tumor xenograft

Ten female BALB/c Nude mice were randomly divided into two groups (n = 5 per group). Skov3 spheroids (1×10^6) transfected with short-hairpin RNA or negative control were injected subcutaneously into the right flank of mice. Administration was performed every 7days for 28 days. Tumor growth was measured through calipers, and tumor weight and volumes were in record. Tumor volumes were calculated according to the formula 0.5 × length × $width^2$.

QUANTIFICATION AND STATISTICAL ANALYSIS

Data are presented as means ± standard error of mean (S.E.). Analysis of significances was done using $\chi 2$ test or, alternately, unpaired Student's t test, two-sided. Significance levels (P values) are indicated in legends of each figure, showing *, $p < 0.05$; **, $p < 0.01$; ***, $p < 0.001$; ****, $p < 0.0001$; n.s., non-significant. All results of *in vitro* experiments were collected from at least 3 independent biological replicates.